Journal of Materials Chemistry A

ROYAL SOCIETY OF CHEMISTRY

PAPER

View Article Online
View Journal | View Issue

Check for updates

Cite this: J. Mater. Chem. A, 2025, 13, 13175

Scalable assembly of flexible ultrathin all-in-one MXene-based supercapacitors†

Zifang Zhao,[a] Zhilong Xu,[a] Yalei Wang,*[bc] Weifeng Huang,[a] Yinfeng Cheng[a] and Wai-Yeung Wong*[c]

Received 13th January 2025
Accepted 18th March 2025

DOI: 10.1039/d5ta00327j

rsc.li/materials-a

Supercapacitors are promising candidates for flexible energy storage devices as a result of their long cycle life and high power density. However, their scalable assembly is still challenging. Herein, a facile blade coating method is employed to realize the fabrication of flexible ultrathin supercapacitors with an integrated all-in-one configuration. The assembly of such supercapacitors can be easily scaled up by adjusting the area of substrates. The all-in-one structure effectively integrates two MXene electrodes, a gel electrolyte and a separator. As a result, they can not only enhance ion- and electronic-transfer capability, but also avoid the slippage or separation between adjacent components under frequent external strain. Moreover, owing to the unique physical and chemical properties of the MXene electrode as well as the structure and electrochemical stability of the integrated all-in-one configuration, the resulting supercapacitors exhibit excellent electrochemical properties, such as a high specific areal capacitance of 77.25 mF cm^{-2} at 2 mV s^{-1}, a long cycle life of 16 000 cycles at 2 A g^{-1}, high rate ability and superior electrochemical stability even under varied bending states.

1. Introduction

The recent boom in flexible electronic technology has promoted the development and production of flexible energy storage devices.[1–5] Among the various flexible energy storage devices, supercapacitors (SCs) are considered as promising candidates as a result of their long cycle life and high power density.[6–11] However, limited by electrode preparation and device design processes, the assembly of flexible SCs is still a challenge.[12–14] Recently, free-standing electrode materials have been widely used in flexible SCs because of the superior mechanical and electrochemical performance. Among various free-standing materials, MXenes have been widely utilized in flexible SCs as a result of their excellent physical properties including surface hydrophobicity, large specific surface area, and metallic conductivity.[15–18] Nevertheless, the reported flexible MXene-based SCs are still mainly assembled into conventional sandwich-stacked structures.[19–21] Since the components of these flexible sandwich-stacked SCs are independent, relative displacement between adjacent components may easily occur and some components or even the whole device may fracture when these devices are exposed to frequent external strain. Thus, serious electrochemical performance degradation may take place. In addition, the bulky architecture of sandwich-stacked SCs limits their further application in flexible electronic devices. Thus, flexible SCs with novel device structures should be further developed.

In comparison with conventional sandwich-stacked SCs, integrated SCs with an all-in-one configuration are favored due to their excellent structural stability.[22] In all-in-one SCs, the electrode, separator, current collector, and other components of the device are integrated together. The seamless connection between adjacent components not only ensures effective ion- and electronic-transfer capability, but also avoids relative slippage and separation between adjacent components under frequent external deformation, thereby improving the mechanical and electrochemical stability of the device.[23–27] Moreover, all-in-one SCs can also reduce their thickness by simplifying the device structure, which helps improve device flexibility and electrochemical performance. The electrodes of flexible all-in-one SCs are generally prepared by depositing or coating active materials onto flexible current collectors.[28,29] Owing to the use of current collectors, ultrathin all-in-one SCs are hard to realize. Meanwhile, the corresponding assembly methods are also challenging to scale up. Consequently, methods to achieve the scalable assembly of flexible ultrathin all-in-one SCs should be developed. Porous cellulose paper is

[a]Xinxiang Key Laboratory of Power Battery Key Technology and Resource Recycling, School of Chemistry and Chemical Engineering, Henan Institute of Science and Technology, Xinxiang 453003, P. R. China

[b]State Key Laboratory of Radio Frequency Heterogeneous Integration, College of Physics and Optoelectronic, Engineering, Key Laboratory of Optoelectronic Devices and Systems of Ministry of Education and Guangdong Province, Shenzhen University, Shenzhen 518060, P. R. China

[c]Department of Applied Biology and Chemical Technology and Research Institute for Smart Energy, The Hong Kong Polytechnic University, Hung Hom, Hong Kong, P. R. China

† Electronic supplementary information (ESI) available. See DOI: https://doi.org/10.1039/d5ta00327j

usually used as the separator in traditional SCs. Because of its flexibility, it could also serve as a flexible substrate for electrodes and buffer internal stress under external deformation. If all components of SCs could be integrated with the cellulose paper, flexible ultrathin SCs with an all-in-one configuration will be realized.

Inspired by this, a scalable assembly method was developed to prepare flexible ultrathin all-in-one MXene-based SCs with all components continuously and seamlessly integrated with a piece of cellulose paper by a facile blade coating method. The assembly of the resulting all-in-one SCs can be easily scaled up by adjusting the area of cellulose paper. Furthermore, with such an all-in-one configuration, the device can not only shorten the ion transfer distance and reduce interfacial contact resistance, but also avoid relative slip and separation between adjacent interfaces under external strain, thus ensuring effective electron- and ion-transfer. As a result, the all-in-one SCs demonstrate high flexibility and excellent electrochemical stability under different external strains.

2. Results and discussion

Fig. 1a schematically shows the assembly process of flexible ultrathin all-in-one SCs. In our case, owing to the superior physical properties such as large surface area, high conductivity, excellent mechanical properties and so on, $Ti_3C_2T_x$ MXene (where T represents terminated groups such as –O, –OH, and –F generated from the etching processes) was selected to serve as the active material for flexible all-in-one SCs. A well-dispersed $Ti_3C_2T_x$ MXene suspension was first prepared by selectively etching the Al layer in Ti_3AlC_2 ceramic material using LiF and HCl. The raw Ti_3AlC_2 consists of bulk particles with size ranging from several microns to tens of microns (Fig. S1†). After etching and sonication treatment, a uniformly dispersed $Ti_3C_2T_x$ suspension was obtained (Fig. S2 and S3†). The structural evolution during this process is reflected in their X-ray diffraction (XRD) plots (Fig. 2a). The Ti_3AlC_2 XRD plot reveals typical Ti_3AlC_2 phase peaks according to the standard spectrum (JCPDS 52-0875). After etching, the strong XRD peaks corresponding to (101), (103), (104), (105) and (107) planes disappeared. Moreover, a distinct shift in the (002) peak from 9.5° to 7.2° is observed, suggesting an increase in the interlayer spacing.[30–32] All these results indicate the successful removal of the Al layer from Ti_3AlC_2. In order to inspect the morphology of MXene, scanning electron microscopy (SEM) and transmission electron microscopy (TEM) were carried out. SEM images of freeze dried $Ti_3C_2T_x$ exhibit a porous structure composed of $Ti_3C_2T_x$ sheets (Fig. 2b and c). TEM shows their flat feature with wrinkling sheets (Fig. 2d). In addition, atomic force microscopy (AFM) characterization was further performed to verify that the obtained $Ti_3C_2T_x$ MXene suspension consisted of MXene sheets with a single layer without restacking (Fig. 2e and f). As can be

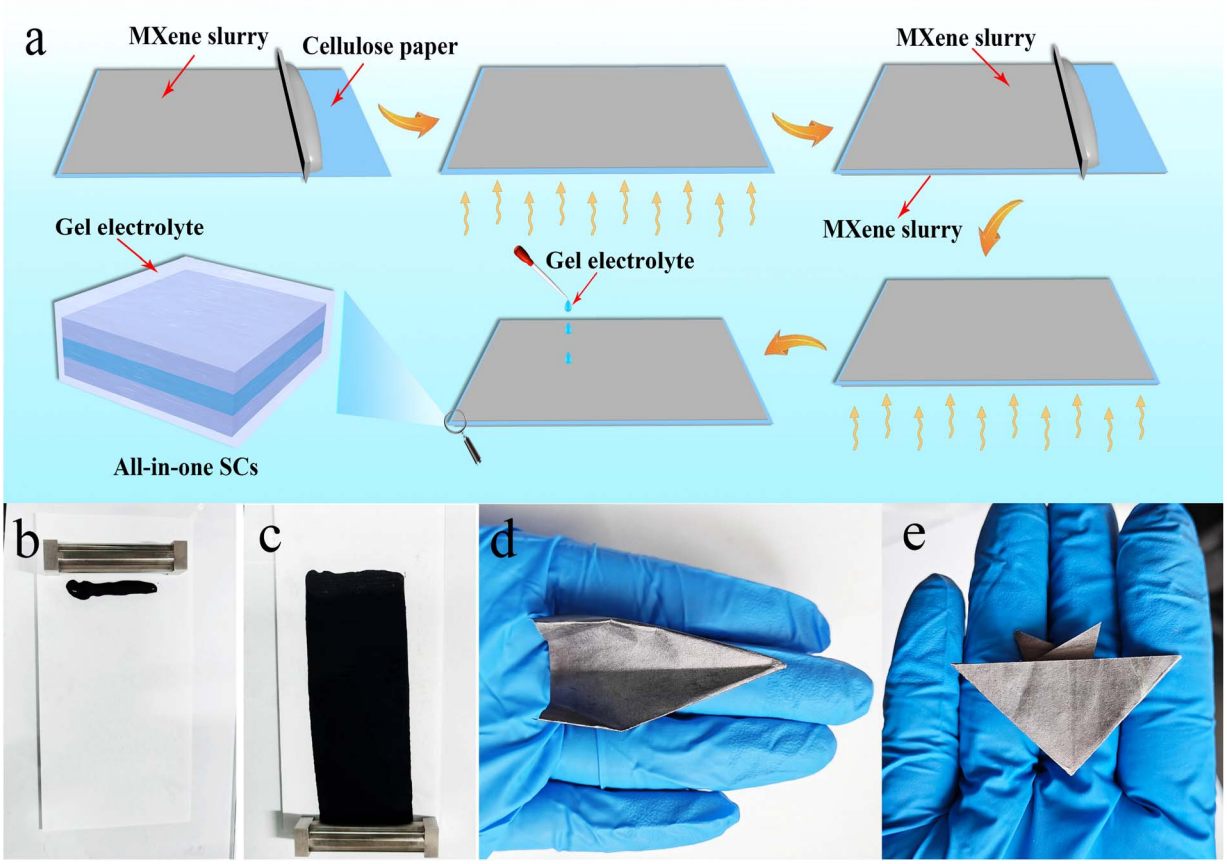

Fig. 1 (a) Schematic illustration of the assembly process of flexible ultrathin all-in-one SCs. (b and c) Photographs showing the blade coating processes. (d and e) Optical images of the flexible ultrathin all-in-one structure.

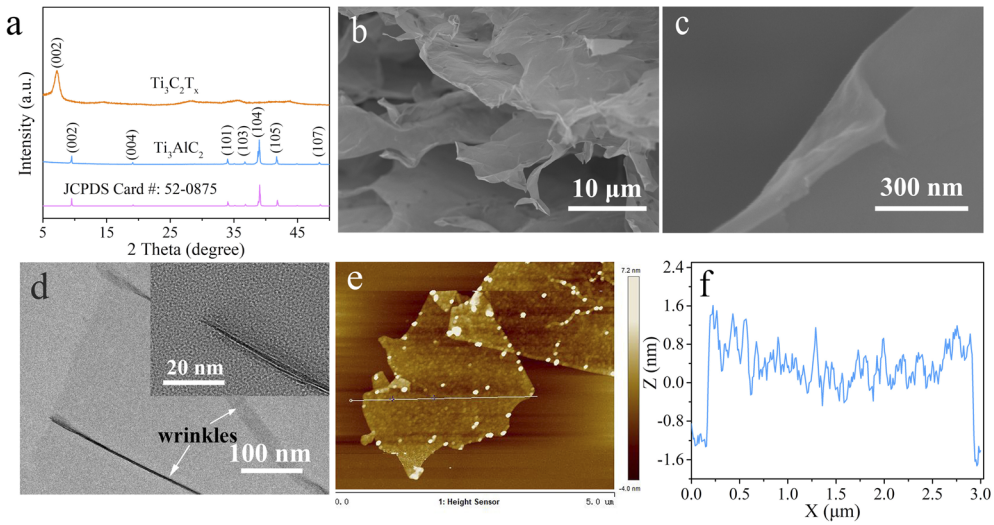

Fig. 2 (a) XRD plots of Ti_3AlC_2 and $Ti_3C_2T_x$ samples. (b and c) SEM images of the freeze-dried $Ti_3C_2T_x$ MXene. (d) TEM image of $Ti_3C_2T_x$ flakes. (e) The AFM image of $Ti_3C_2T_x$ sheets. (f) The thickness curve of $Ti_3C_2T_x$ sheets received from the AFM image.

seen, the size of $Ti_3C_2T_x$ MXene sheets lies within several microns with a thickness of about 1.65 nm. As the theoretical thickness of a $Ti_3C_2T_x$ MXene monolayer is approximately 1 nm, and considering factors such as surface functional groups and the adsorption of water or other contaminants that may increase the thickness, it can be inferred that the $Ti_3C_2T_x$ MXene suspension obtained in the experiment primarily comprised single-layer $Ti_3C_2T_x$ MXene sheets, and the restacking of the $Ti_3C_2T_x$ MXene sheets was prevented.[33–35]

In a typical experiment, the $Ti_3C_2T_x$ MXene slurry with a concentration of ~26 mg mL^{-1} was directly coated onto both sides of a piece of cellulose paper through a blade coating process, obtaining the ultrathin MXene film-separator-MXene film all-in-one structure (Fig. 1b–e and S4†). After that, a gel electrolyte was added to the structure, achieving the ultrathin all-in-one SCs. In order to validate the versatility of this method, the same MXene slurry was also blade coated onto various substrates, including Celgard 2400, filter paper, and glass fiber. Multimeter measurements revealed infinite bilateral resistance across all integrated structures, indicating that the MXene slurry did not permeate these substrates and this blade coating method works with both cellulose and noncellulose substrates (Fig. S5†). Besides, we also conducted repeated 1000 stretching and bending experiments (stretching to a flat state followed by bending until the distance between the two ends of the material reached zero) on a stretching platform to evaluate potential degradation over extended mechanical cycling. Initial SEM images of the electrode surface reveal flat and intact features (Fig. S6†). After 500 bending cycles, minor cracks began to appear on the surface. These cracks became more pronounced after 1000 bending cycles. Despite this, no macroscopic cracks that could compromise the structural integrity were observed, demonstrating excellent mechanical properties.

The surface of MXene films coated on the cellulose paper exhibits a densely packed structure composed of two-dimensional MXene sheets (Fig. 4a and b). The thickness of the all-in-one structure is less than 100 μm, approximating the thickness of a veil, as reflected by the SEM images and corresponding elemental mappings (Fig. 4c–f). In addition, the MXene layer with a thickness of approximately 4.5 μm adheres to both sides of the cellulose paper separator. In such an all-in-one structure, the $Ti_3C_2T_x$ film electrodes can be firmly connected with the neighboring cellulose paper separator, displaying a continuous connection between the electrodes and separator. Impressively, as the blade coating method only involves coating MXene slurry on cellulose paper, there is no limit to the size of MXene films as well as the cellulose paper. Therefore, the preparation of MXene-based flexible ultrathin all-in-one SCs can be scaled up easily.

Since the electrochemical performance of $Ti_3C_2T_x$ depends largely on the type and content of their terminated groups,[36] X-ray photoelectron spectroscopy (XPS) was conducted to analyze chemical bonding of their terminated groups (Fig. 3a–e). The XPS survey spectrum of $Ti_3C_2T_x$ indicates the presence of Ti, C, O, and F elements (Fig. 3a). The C 1s spectrum of $Ti_3C_2T_x$ is divided into three fitting peaks (Fig. 3b). The peaks centered at 282.5, 284.8 and 286.8 eV are ascribed to C–Ti, C–C/C=C, and C–O, respectively. Fig. 3c presents the Ti 2p spectrum of $Ti_3C_2T_x$ MXene, showcasing peaks corresponding to Ti–C, Ti^{2+}, and Ti^{3+}. These findings align well with earlier studies.[37,38] Notably, there are no deconvoluted peaks indicative of TiO_2, suggesting that the $Ti_3C_2T_x$ MXene remained unoxidized throughout the synthesis process. The XPS O 1s spectrum of $Ti_3C_2T_x$ shows four fitting peaks of C–Ti–O_x, Ti–O, C–Ti–$(OH)_x$ and H_2O at 532.6, 533.0, 534.3 and 536.0 eV, respectively (Fig. 3d). In the F 1s region of the $Ti_3C_2T_x$ MXene sample, the primary component is C–Ti–F_x bond at 685.1 eV (Fig. 3e). The presence of Al–F_x is minimal, suggesting that Al has been effectively removed. These results confirm the successful synthesis of $Ti_3C_2T_x$ MXene and indicate that the surface of $Ti_3C_2T_x$ MXene is rich in oxygen-containing functional groups, which can provide significant

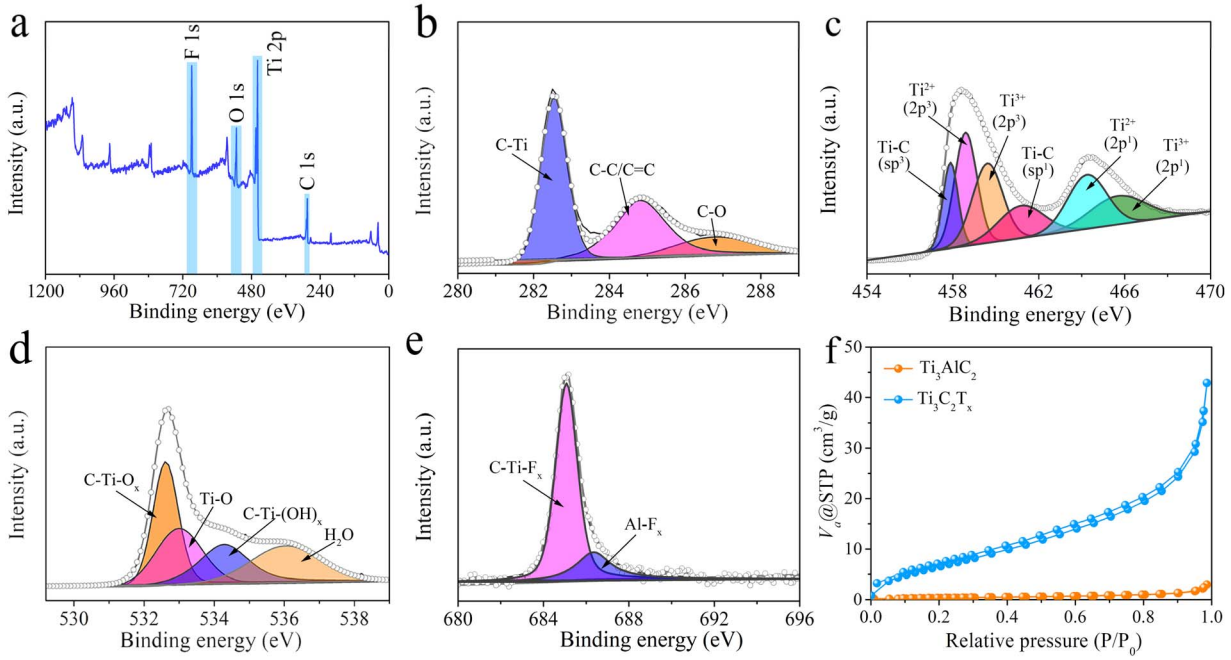

Fig. 3 (a) XPS survey spectrum of $Ti_3C_2T_x$. High resolution (b) C 1s, (c) Ti 2p, (d) O 1s, and (e) F 1s spectra of $Ti_3C_2T_x$. (f) N_2 adsorption/desorption curves of Ti_3AlC_2 and $Ti_3C_2T_x$.

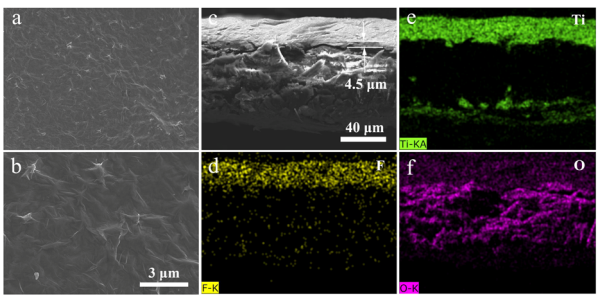

Fig. 4 (a and b) SEM images of the MXene film coating on a piece of cellulose paper. (c–f) Cross-sectional SEM image and the corresponding elemental mappings of the integrated structure.

pseudocapacitance to the $Ti_3C_2T_x$ electrode, thus contributing to the improved electrochemical performance of SCs based on them.

Apart from the terminated groups, a large specific surface area is also required to meet the high energy density demand. As a result, a N_2 adsorption–desorption isotherm was further performed to evaluate the specific surface area of $Ti_3C_2T_x$ (Fig. 3f). Significantly, a type-II isotherm is observed in $Ti_3C_2T_x$ samples, corresponding to a single–multilayer reversible adsorption process occurring on the non-porous solid or macroporous solid surface. This indicates the existence of a macropore structure, which is consistent with the SEM results (Fig. 2b). The adsorption and desorption curve of Ti_3AlC_2 is a type III isotherm without an inflection point, corresponding to the multimolecular layer adsorption process on the hydrophobic surface, where the adsorption interaction between the solid and adsorbate is weaker than the interaction between adsorbate molecules. The specific surface area of Ti_3AlC_2 and $Ti_3C_2T_x$ is 1.97 $m^2\ g^{-1}$ and 28.12 $m^2\ g^{-1}$, respectively. The Barrett–Joyner–Halenda (BJH) analysis (Fig. S7†) reveals that the pore volume of $Ti_3C_2T_x$ MXene is 0.066 $cm^3\ g^{-1}$, almost 15 times larger than that (0.0045 $cm^3\ g^{-1}$) of Ti_3AlC_2. The pore size distribution of $Ti_3C_2T_x$ primarily concentrates within the range of 1–16 nm, with a peak at 1.88 nm. However, due to the limitations of test conditions, the pore size distribution analysis of macropore structures is restricted. These results indicate that the surface area of $Ti_3C_2T_x$ is greatly improved after etching of Ti_3AlC_2 with HCl and LiF, and the $Ti_3C_2T_x$ material contains a significant number of micropores and mesopores.

Owing to its excellent electrical conductivity, abundant terminated groups, and large surface area, $Ti_3C_2T_x$ is a good electrode candidate for SCs. For the purpose of understanding the electrochemical performance of $Ti_3C_2T_x$ electrodes, SCs based on the all-in-one structure were fabricated with 1.0 mol per L H_2SO_4 electrolyte. Typical rectangle-like cyclic voltammetry (CV) curves were obtained even at a high scan rate of 200 mV s^{-1} (Fig. 5a), suggesting the superior rate capability. It is also demonstrated by their isosceles triangle shaped galvanostatic charge/discharge (GCD) curves (Fig. 5c). Moreover, as the scan rate increases by 100 times (2–200 mV s^{-1}), the specific capacitance of the $Ti_3C_2T_x$ MXene films retains 68% of its initial value (177.5–121.1 mF cm^{-2}, for a single electrode) as shown in Fig. 5b, indicating their excellent rate performance.

Besides high electrical conductivity, abundant terminated groups, and large surface area, $Ti_3C_2T_x$ also possesses excellent mechanical performance. Therefore, it can serve as flexible electrodes for all-in-one SCs. Based on $Ti_3C_2T_x$, flexible all-in-one SCs were fabricated with PVA/H_2SO_4 gel electrolyte, as depicted in Fig. 5d. Typical rectangle-like CV curves of all-in-one

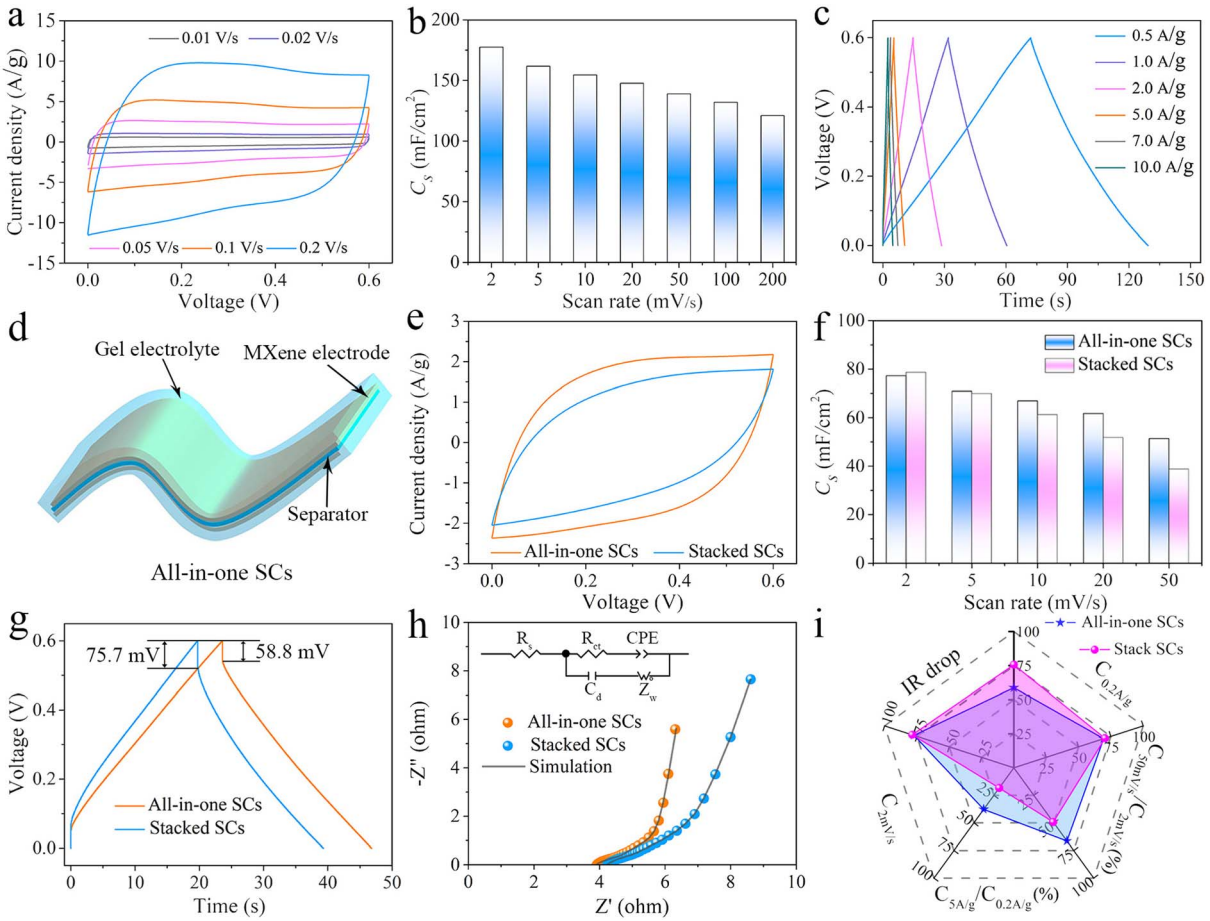

Fig. 5 (a–c) The electrochemical performance of the SCs with 1.0 mol per L H_2SO_4 electrolyte: (a) CV curves at different scan rates; (b) the corresponding areal capacitances at different scan rates; (c) GCD plots at varying current densities. (d) Schematic diagram of the fabricated flexible all-in-one SCs. (e–i) Electrochemical performance of SCs with all-in-one and stacked structures: (e) CV curves at 50 mV s^{-1}; (f) areal capacitances depend on scan rates; (g) GCD curves at 1 A g^{-1}; (h) Nyquist curves (100 mHz–100 kHz); (i) comparison of the electrochemical performance between all-in-one and stacked SCs.

SCs indicate the low electrical resistance and excellent reversibility during the charging/discharging process of the flexible all-in-one SCs (Fig. 5e). The specific capacitance of the flexible all-in-one SCs is calculated to be 77.25 mF cm^{-2} at 2 mV s^{-1}, which is comparable to those of stacked SCs (Fig. 5f) and the reported flexible supercapacitors prepared by spay/blade coating methods (Fig. S8†).[39–44] Moreover, they can still deliver a high specific capacitance of 51.35 mF cm^{-2} even at a high scan rate of 50 mV s^{-1}. In contrast, the stacked SCs at the same scan rates suffer from more serious capacitance damping (Fig. 5f). These results are also supported by their GCD curves at 1 A g^{-1} (Fig. S9†). In addition, the IR drop (58.8 mV) of the all-in-one SCs is also less than that of the stacked SCs (75.7 mV), demonstrating lower internal resistance of the flexible all-in-one SCs (Fig. 5g). Such an excellent rate performance is attributed to their shorter ion diffusion distance and faster electrochemical reaction kinetics, which is revealed by the electrochemical impedance spectroscopy (EIS) results (Fig. 5h). The measured Nyquist plots are fitted to an equivalent circuit (inset in Fig. 5h), and the fitting parameters are listed in Table S1† in the ESI.† In the high frequency region, all-in-one SCs show smaller internal resistance (R_s, 2.737 Ω) and charge-transfer impedance (R_{ct}, 3.864 Ω) than the stacked SCs. Furthermore, from the relationship between Z' and $\omega^{-1/2}$ ($\omega = 2\pi f$) in the low frequency region (Fig. S10†), the all-in-one SCs show a lower slope, indicating their smaller charge transfer resistance and ion diffusion kinetics.[45] The excellent kinetics of the all-in-one device could be ascribed to the seamless connection between neighboring components, which provides a continuous electron-/ion-transfer pathway. Therefore, all-in-one SCs show superior electrochemical performance compared to the stacked SCs (Fig. 5i).

Fig. 6a shows the CV curves of flexible all-in-one SCs based on $Ti_3C_2T_x$ at 2–50 mV s^{-1}. The rectangle-like CV curves even at high scan rates imply their excellent capacitive behavior. Besides, current responses of the all-in-one SCs exhibit a nearly linear connection with scan rates (Fig. 6b), evidencing the superior rate performance. With these excellent electrochemical properties, the all-in-one SCs can be charged and discharged over a wide current density ranging from 0.2 to 2 A g^{-1} and nearly triangular shaped GCD plots can be achieved (Fig. 6c). In contrast, CV and GCD curves of the stacked SCs were shown in

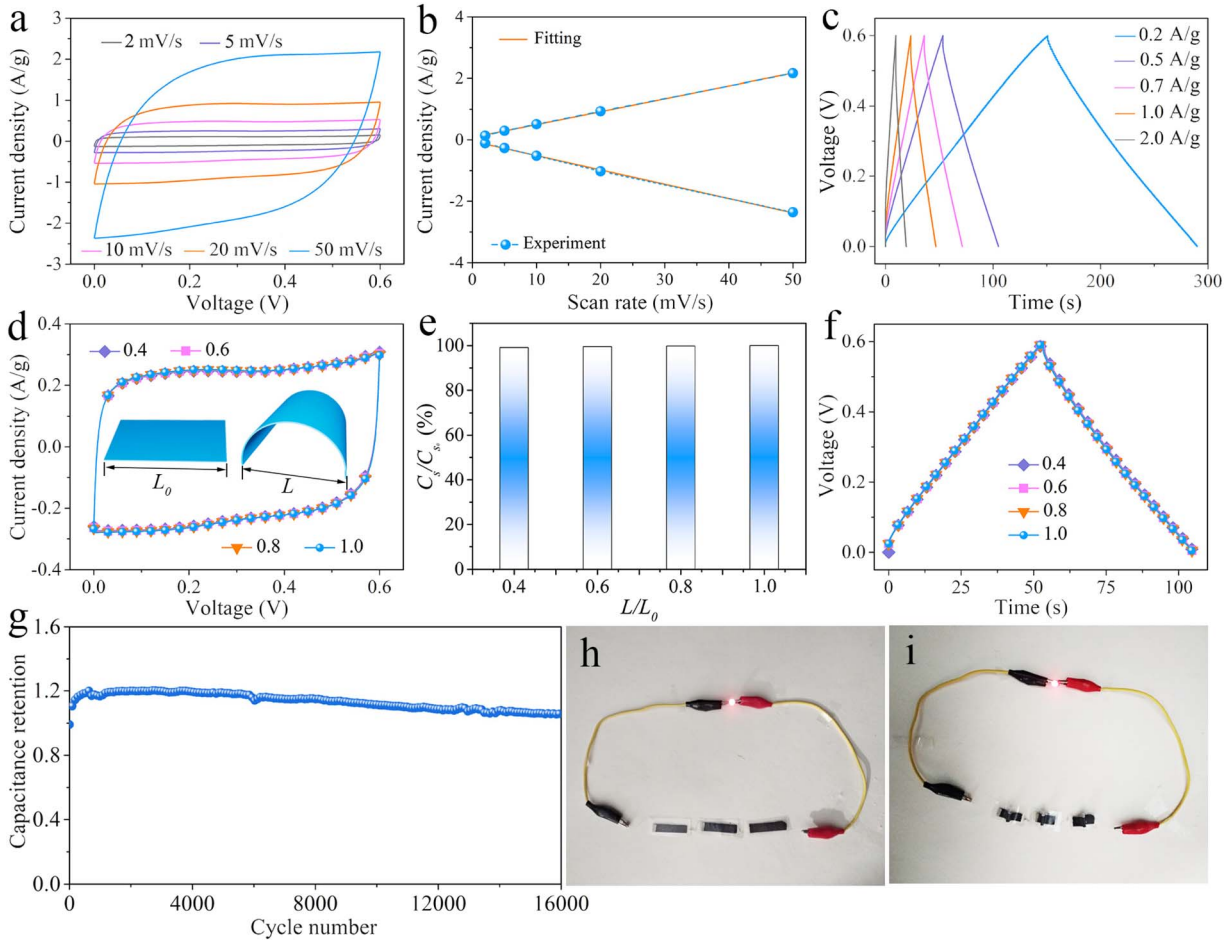

Fig. 6 (a–g) Electrochemical properties of flexible all-in-one SCs: (a) CV curves, (b) current responses of CV curves, (c) GCD plots, (d) CV curves at 5 mV s^{-1}, (e) normalized specific capacitances based on CV curves and (f) GCD plots at 0.5 A g^{-1} at varying L/L_0 values (C_{s_0} and L_0 represent the initial capacitance and the length of all-in-one SCs, C_s and L are capacitances and lengths under bending states), (g) cycling performance, (h and i) optical photographs of an LED lighted by all-in-one devices in series under (h) flat and (i) bending states.

Fig. S11.† For the purpose of certifying stable electrochemical performance of all-in-one SCs, CV curves at different bending states (flat state as well as bent it to 40% (1.2 cm), 60% (1.8 cm), and 80% (2.4 cm) of its original length (3 cm)) were obtained (Fig. 6d). Little distinction is observed in the CV curves and their corresponding normalized capacitances under different bending states (Fig. 6e), suggesting the high electrochemical stability of the flexible all-in-one SCs. The stability of all-in-one SCs can be also suggested by their GCD plots at different bending states (Fig. 6f). In addition, cycle performance is another important factor for the applications of flexible devices. The capacitance retention of all-in-one SCs kept increasing during the initial 650 cycles. This can be attributed to the gradually improved electrolyte accessibility to the active sites resulting from the increased interlayer spacing during the cycling process.[46–48] After the initial 650 cycles, only a slight capacity fade is observed over the subsequent 15 350 cycles at 2 A g^{-1} (Fig. 6g), indicating their superior cycling stability. Such excellent electrochemical performance makes our flexible all-in-one SCs promising for use as flexible power sources. To demonstrate the flexibility of our all-in-one SCs visually, three devices under flat and bending states in series were connected to light an LED (Fig. 6h and i). The nearly unchanged brightness of an LED indicates the applicability and compatibility of the devices as flexible energy storage devices for portable electronics.

The excellent electrochemical performance of flexible all-in-one SCs depends on their fast electrochemical reaction kinetics, which can be reflected in their CV curves (Fig. 6a). The current (i) in the CV curves can be usually considered as the sum of the surface capacitance control current (i_{cap}) and the diffusion control current (i_{diff}), and its empirical formula is as follows:[49]

$$i = i_{cap} + i_{diff} = av^b \quad (1)$$

or rewritten as:

$$\log(i) = b\log(v) + \log(a) \quad (2)$$

where v is the scan rate, and a and b are adjustable parameters. When b approaches 0.5, the electrochemical reaction becomes diffusion-controlled, and when b approaches 1.0, surface capacitance control with a quick kinetic behavior dominates the

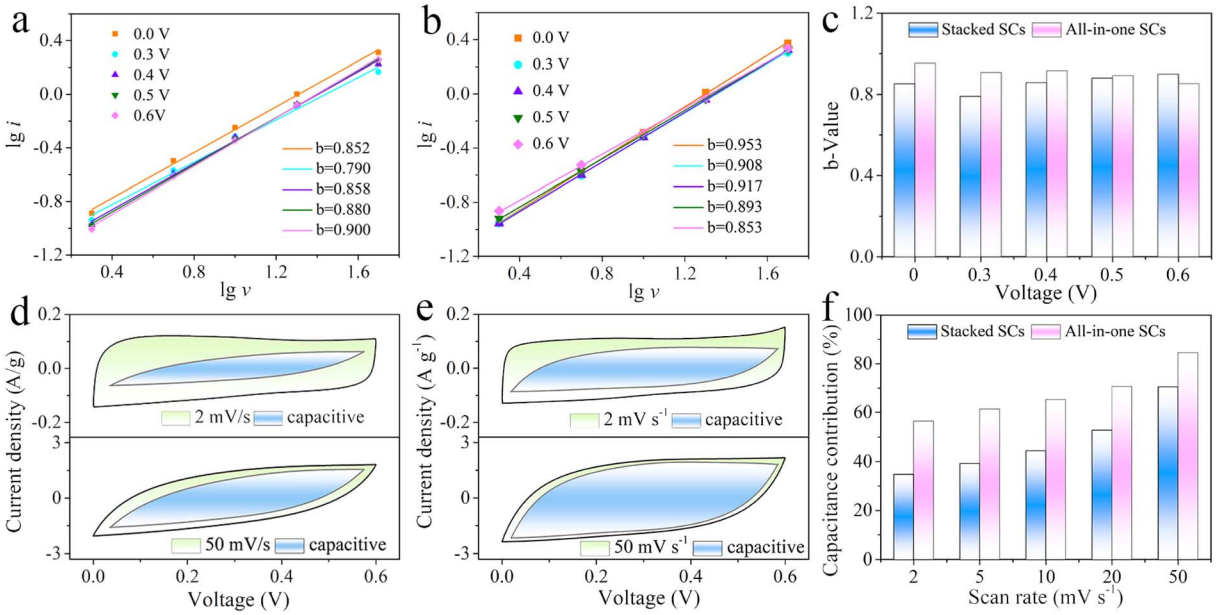

Fig. 7 The electrochemical reaction kinetic analysis of the flexible all-in-one SCs during the charge/discharge process: the fitted plots of lg *i* *versus* lg *v* at different potentials: (a) stacked SCs and (b) all-in-one SCs. (c) The variation in *b*-values of all-in-one and stacked SCs under different potentials. CV curves of stacked SCs with a capacitance contribution at 2 and 50 mV s^{-1}, respectively: (d) stacked SCs, (e) all-in-one SCs. (f) Capacitance contribution comparison of all-in-one SCs with stacked SCs at various scan rates.

entire electrochemical reaction. According to eqn (2), the plots of lg *v* *versus* lg *i* were linearly fitted as shown in Fig. 7a and b. The *b* values of the all-in-one SCs range from 0.853 to 0.953, while those of the stacked SCs range from 0.790 to 0.900 under different potentials, revealing that the electrochemical reaction in both all-in-one and stacked SCs is mainly dominated by the surface capacitance control (Fig. 7c). However, the higher *b* values of all-in-one SCs indicate much faster electrochemical kinetics compared to stacked SCs.

A quantitative analysis of the capacitance contribution percentage was further conducted by Dunn's method.[50] The current at specific potentials can be described as follows:[51]

$$i = k_1 v + k_2 v^{1/2} \quad (3)$$

where v is the scan rate, values $k_1 v$ and $k_2 v^{1/2}$ represent the contributions of the surface capacitance control process and diffusion process to total current (i), respectively. The contributions of surface capacitance can be distributed in the form of the area in the CV curves (Fig. 7d and e). The capacitance contributions increase gradually with increasing scan rates, indicating that high scan rates are beneficial to the capacitance contribution, as the ion insertion/deintercalation process at high scan rates is confined to surface charging/discharging. Besides, the capacitance contributions of all-in-one SCs at 2, 5, 10, 20 and 50 mV s^{-1} were calculated to be 56.42%, 61.33%, 65.28%, 70.63% and 84.53%, respectively, which are higher than those of the stacked SCs at the same scan rates (Fig. 7f). This result is consistent with the rate performance results (Fig. 5f), and it may be ascribed to the enhanced electron and/or load transfer capability of all-in-one SCs. Therefore, the all-in-one SCs exhibit faster charge transfer kinetics than the stacked SCs.

3. Conclusions

In summary, flexible ultrathin all-in-one MXene-based SCs were designed and successfully prepared through a scalable blade coating strategy, which effectively integrated the two MXene electrodes, a gel electrolyte and a separator in a single structure. The continuous interlayer connection can effectively avoid the sliding or relative separation of adjacent components under external mechanical deformation, thus ensuring stable ion- and electron-transfer ability. Therefore, the integrated all-in-one SCs show fast electrochemical reaction kinetics as well as excellent flexibility and structural stability even under varied bending states. The scalable strategy developed here provides a new idea of assembling all components of SCs into all-in-one structures with remarkable structural and electrochemical stability.

4. Experimental

4.1 Preparation of MXene

$Ti_3C_2T_x$ MXene was prepared by exfoliating the Ti_3AlC_2 MAX phase through the LiF/HCl etching strategy. In a typical process, 2 g LiF powder (Alfa Aesar) was first added into 40 mL of 6 mol L^{-1} HCl and the mixture was stirred for 10 minutes to dissolve the salt. After that, 2 g of Ti_3AlC_2 MAX phase was added to the solution which was kept at 45 °C for 3 days under continuous stirring. Subsequently, the obtained mixture was washed with deionized water until pH of the washing water reached approximately 6 and sediment was collected. Next, 300 mL deionized water was added to the above sediment and the mixture was stirred for 12 hours. After 30 minutes of sonication and 30 minutes of centrifugation treatment at 3500 r min^{-1}, the uniformly dispersed $Ti_3C_2T_x$ suspension was obtained.

4.2 Assembly of flexible ultrathin all-in-one MXene-based SCs

The well-dispersed $Ti_3C_2T_x$ MXene suspension was first subjected to high-speed centrifugation to obtain a concentrated MXene slurry. The concentration of the MXene slurry was adjusted to ~26 mg mL^{-1} with absolute ethanol serving as the dispersing agent. It was directly utilized as the electrode materials for flexible ultrathin all-in-one SCs. Then, 1 g concentrated H_2SO_4 and 10 mL deionized water were mixed uniformly. 1 g poly(vinyl alcohol) (PVA) was added to the above H_2SO_4 solution afterwards. The whole mixture was then heated to 85 °C under continuous stirring until it became clear, obtaining a PVA/H_2SO_4 gel electrolyte. After that, the MXene slurry was coated onto a piece of clean cellulose paper with the coating thickness precisely controlled at 200 μm using a doctor blade. In order to avoid stress concentration and cracking during the drying process, a staged drying method was employed, with room temperature drying for 2 hours to remove most of the solvent followed by vacuum drying at 60 °C for 12 hours to obtain the MXene–cellulose paper. The active material loading on one side was 0.75 mg cm^{-2}. Then, the same method was used to coat MXene slurry on the other side of the cellulose paper to obtain the MXene–cellulose paper-MXene integrated all-in-one structure. Finally, 100 μL of the hot PVA/H_2SO_4 electrolyte was added dropwise to the all-in-one structure (cut into a size of 3 × 1 cm^2) and dried under vacuum, achieving the assembly of flexible ultrathin all-in-one MXene-based SCs.

4.3 Assembly of flexible stacked MXene-based SCs

The MXene electrodes of stacked MXene-based SCs were prepared by blade coating the same MXene slurry (~26 mg mL^{-1}) on the commercial polypropylene membrane (Celgard 2400) with a coating thickness of 200 μm. After the drying process, free-standing MXene films were peeled off from the polypropylene membrane. A piece of cellulose paper and 100 μL of the hot PVA/H_2SO_4 solution were used as the separator and gel electrolyte, respectively. The flexible stacked SCs were fabricated by sandwiching the cellulose paper with two pieces of identical MXene films, each peeled off from the polypropylene membrane (cut into a size of 3 × 1 cm^2).

4.4 Material characterization

The morphology of materials and all-in-one devices was characterized by scanning electron microscopy (SEM, Regulus8220) and transmission electron microscopy (TEM, FEI Talos F200X G2). Atomic force microscopy (AFM, Bruker Dimension ICON) was employed to characterize the morphology and thickness of MXene sheets. The crystal structure of materials was characterized by X-ray diffraction (XRD, DX-27008). Element type and valence information of the sample were characterized by X-ray photoelectron spectroscopy (XPS, PHI 1600 ESCA). The specific surface area of the material was measured using a nitrogen adsorption isotherm tester (ASAP 2020).

4.5 Electrochemical tests

The GCD and CV curves were measured on a CHI660E electrochemical workstation. The cyclic performance of SCs was carried out on an Arbin supercapacitor test system (BT 2000). The specific areal capacitance (C_s) of all-in-one devices *versus* current densities and scan rates are calculated with the formulae given below:

$$C_s = \frac{i\Delta t}{s\Delta V} (versus \text{ current densities}) \quad (4)$$

$$C_s = \frac{\int I \mathrm{d}V}{2sv\Delta V} (versus \text{ scan rates}) \quad (5)$$

where i (A) is the discharge current, Δt (s) is the discharge time, ΔV is the potential window, s (cm^2) is the area of all-in-one devices, I (A) is the current during cyclic voltammetry tests and v (V s^{-1}) is the scan rate. EIS was carried out over a frequency range of 100 mHz–100 kHz on the same CHI660E electrochemical workstation with an amplitude of 5 mV.

Data availability

The data are available from the corresponding author on reasonable request.

Author contributions

Zifang Zhao: conceptualization, data curation, funding acquisition, writing – original draft, writing – review & editing; Zhilong Xu: project administration, writing – original draft; Yalei Wang: conceptualization, formal analysis, writing – review & editing; Weifeng Huang: formal analysis, investigation, methodology; Yinfeng Cheng: supervision, project administration; Wai-Yeung Wong: funding acquisition, resources, conceptualization.

Conflicts of interest

There are no conflicts to declare.

Acknowledgements

This work was supported by the National Natural Science Foundation of China (No. 52102268 and 22309044), the RGC Senior Research Fellowship Scheme (SRFS2021-5S01), the Hong Kong Research Grants Council (PolyU 15307321), the Research Institute for Smart Energy (CDAQ), the Research Centre for Nanoscience and Nanotechnology (CE2H), and the Research Centre for Carbon-Strategic Catalysis (CE01 and CE2L), as well as by the Endowed Professorship in Energy (847S) funded by Miss Clarea Au, the Key Project of Science and Technology Program of Henan Province (No. 222102240001 and 252102231043), and the Key Scientific Research Project of Colleges and Universities in Henan Province (No. 24B150011).

References

1 X. Xu, S. Xie, Y. Zhang and H. Peng, The Rise of Fiber Electronics, *Angew. Chem., Int. Ed.*, 2019, **58**, 13643–13653, DOI: 10.1002/anie.201902425.

2 D. P. Dubal, N. R. Chodankar, D. H. Kim and P. Gomez-Romero, Towards flexible solid-state supercapacitors for smart and wearable electronics, *Chem. Soc. Rev.*, 2018, **47**, 2065–2129, DOI: 10.1039/c7cs00505a.

3 Q. Xue, J. F. Sun, Y. Huang, M. S. Zhu, Z. X. Pei, H. F. Li, Y. K. Wang, N. Li, H. Y. Zhang and C. Y. Zhi, Recent Progress on Flexible and Wearable Supercapacitors, *Small*, 2017, **13**, 1701827, DOI: 10.1002/smll.201701827.

4 K. Shang, J. Gao, X. Yin, Y. Ding and Z. Wen, An Overview of Flexible Electrode Materials/Substrates for Flexible Electrochemical Energy Storage/Conversion Devices, *Eur. J. Inorg. Chem.*, 2021, **2021**, 606–619, DOI: 10.1002/ejic.202001024.

5 Z. Sun, Z. Ma, X. Zhou, Y. Wang, J. Zhang and W.-Y. Wong, Ferrocene-modified polymer-SWCNT composite films for high-performance flexible thermoelectric generators, *J. Mater. Chem. A*, 2024, **12**, 22061–22069, DOI: 10.1039/D4TA02037E.

6 L. Wu, X. Y. Shi and Z. S. Wu, Recent Advancements and Perspectives of Biodegradable Polymers for Supercapacitors, *Adv. Funct. Mater.*, 2023, **33**, 2211454, DOI: 10.1002/adfm.202211454.

7 H. Gao, B. Joshi, E. Samuel, A. Khadka, S. Wung Kim, A. Aldalbahi, M. El-Newehy and S. S. Yoon, Freestanding electrodes based on nitrogen-doped carbon nanofibers and zeolitic imidazolate framework-derived ZnO for flexible supercapacitors, *Appl. Surf. Sci.*, 2024, **651**, 159221, DOI: 10.1016/j.apsusc.2023.159221.

8 Z. F. Zhao, X. J. Wang, M. J. Yao, L. L. Liu, Z. Q. Niu and J. Chen, Activated carbon felts with exfoliated graphene nanosheets for flexible all-solid-state supercapacitors, *Chin. Chem. Lett.*, 2019, **30**, 915–918, DOI: 10.1016/j.cclet.2019.03.003.

9 Y. M. Wang, X. L. Wu, Y. Q. Han and T. X. Li, Flexible supercapacitor: Overview and outlooks, *J. Energy Storage*, 2021, **42**, 103053, DOI: 10.1016/j.est.2021.103053.

10 Z. Shi, G. Sun, R. Yuan, W. Chen, Z. Wang, L. Zhang, K. Zhan, M. Zhu, J. Yang and B. Zhao, Scalable fabrication of $NiCo_2O_4$/reduced graphene oxide composites by ultrasonic spray as binder-free electrodes for supercapacitors with ultralong lifetime, *J. Mater. Sci. Technol.*, 2022, **99**, 260–269, DOI: 10.1016/j.jmst.2021.05.040.

11 W. Li, C. Li, Y. Xu, G. Wang, T. Xu, W. Zhang and C. Si, Heteroatom-doped and graphitization-enhanced lignin-derived hierarchically porous carbon via facile assembly of lignin-Fe coordination for high-voltage symmetric supercapacitors, *J. Colloid Interface Sci.*, 2024, **659**, 374–384, DOI: 10.1016/j.jcis.2023.12.162.

12 X. Yin, H. Li, R. Yuan and J. Lu, Metal-organic framework derived hierarchical $NiCo_2O_4$ triangle nanosheet arrays@SiC nanowires network/carbon cloth for flexible hybrid supercapacitors, *J. Mater. Sci. Technol.*, 2021, **81**, 162–174, DOI: 10.1016/j.jmst.2020.10.085.

13 Y. L. Shao, M. F. El-Kady, L. J. Wang, Q. H. Zhang, Y. G. Li, H. Z. Wang, M. F. Mousavi and R. B. Kaner, Graphene-based materials for flexible supercapacitors, *Chem. Soc. Rev.*, 2015, **44**, 3639–3665, DOI: 10.1039/c4cs00316k.

14 X. H. Lu, M. H. Yu, G. M. Wang, Y. X. Tong and Y. Li, Flexible solid-state supercapacitors: design, fabrication and applications, *Energy Environ. Sci.*, 2014, **7**, 2160–2181, DOI: 10.1039/c4ee00960f.

15 Y. Z. Fang, B. W. Yang, D. T. He, H. P. Li, K. Zhu, L. Wu, K. Ye, K. Cheng, J. Yan, G. L. Wang and D. X. Cao, Porous and free-standing $Ti_3C_2T_x$-RGO film with ultrahigh gravimetric capacitance for supercapacitors, *Chin. Chem. Lett.*, 2020, **31**, 1004–1008, DOI: 10.1016/j.cclet.2019.08.043.

16 B. Kalleshappa and M. Pumera, Recyclable HF-free $Ti_3C_2T_x$ 3D-printed supercapacitors: their second life in sodium-ion batteries, *J. Mater. Chem. A*, 2025, **13**, 795–807, DOI: 10.1039/D4TA07436J.

17 Z. F. Zhao, S. Wang, F. Wan, Z. W. Tie and Z. Q. Niu, Scalable 3D Self-Assembly of MXene Films for Flexible Sandwich and Microsized Supercapacitors, *Adv. Funct. Mater.*, 2021, **31**, 2101302, DOI: 10.1002/adfm.202101302.

18 D. Fan, Z. Fang, Z. Xiong, F. Fu, S. Qiu and M. Yan, Self-assembled high polypyrrole loading flexible paper-based electrodes for high-performance supercapacitors, *J. Colloid Interface Sci.*, 2024, **660**, 555–564, DOI: 10.1016/j.jcis.2024.01.031.

19 H. Xu, J. Fan, H. Su, C. Liu, G. Chen, Y. Dall'Agnese and Y. Gao, Metal Ion-Induced Porous MXene for All-Solid-State Flexible Supercapacitors, *Nano Lett.*, 2023, **23**, 283–290, DOI: 10.1021/acs.nanolett.2c04320.

20 P. Liu, H. D. Liu, T. F. Zhang, L. Chen, W. Guo, T. T. Gu, F. Yu, Y. Y. Liu and G. Wang, $Ti_3C_2T_x$ quantum dot-modified $Ti_3C_2T_x$ nanosheets freestanding films for flexible solid-state pseudocapacitors, *Chem. Eng. J.*, 2023, **477**, 146913, DOI: 10.1016/j.cej.2023.146913.

21 Q. Li, X. Guo, Y. Zhang, W. Zhang, C. Ge, L. Zhao, X. Wang, H. Zhang, J. Chen, Z. Wang and L. Sun, Porous graphene paper for supercapacitor applications, *J. Mater. Sci. Technol.*, 2017, **33**, 793–799, DOI: 10.1016/j.jmst.2017.03.018.

22 Z. Yong, S. Wang, X. Wang, G. Liu, D. Liang, Y. Cui, F. Liu, D. Wang and Z. Wang, An all-in-one flexible supercapacitor based on redox ionogel electrolyte with high cycle performance, *J. Alloys Compd.*, 2022, **893**, 162197, DOI: 10.1016/j.jallcom.2021.162197.

23 S. H. Zheng, X. Y. Tang, Z. S. Wu, Y. Z. Tan, S. Wang, C. L. Sun, H. M. Cheng and X. H. Bao, Arbitrary-Shaped Graphene-Based Planar Sandwich Supercapacitors on One Substrate with Enhanced Flexibility and Integration, *ACS Nano*, 2017, **11**, 2171–2179, DOI: 10.1021/acsnano.6b08435.

24 X. Y. Wang, Q. Q. Lu, C. Chen, M. Han, Q. R. Wang, H. X. Li, Z. Q. Niu and J. Chen, A Consecutive Spray Printing Strategy to Construct and Integrate Diverse Supercapacitors on Various Substrates, *ACS Appl. Mater. Interfaces*, 2017, **9**, 28612–28619, DOI: 10.1021/acsami.7b08833.

25 J. M. Du, C. Zheng, W. Lv, Y. Q. Deng, Z. Z. Pan, F. Y. Kang and Q. H. Yang, A Three-Layer All-In-One Flexible Graphene Film Used as an Integrated Supercapacitor, *Adv. Mater. Interfaces*, 2017, **4**, 1700004, DOI: **10.1002/admi.201700004**.

26 Q. R. Wang, X. Y. Wang, F. Wan, K. N. Chen, Z. Q. Niu and J. Chen, An All-Freeze-Casting Strategy to Design Typographical Supercapacitors with Integrated Architectures, *Small*, 2018, **14**, 1800280, DOI: **10.1002/smll.201800280**.

27 D. Wen, G. Ying, L. Liu, Y. Li, C. Sun, C. Hu, Y. Zhao, Z. Ji, J. Zhang and X. Wang, Direct inkjet printing of flexible MXene/graphene composite films for supercapacitor electrodes, *J. Alloys Compd.*, 2022, **900**, 163436, DOI: **10.1016/j.jallcom.2021.163436**.

28 T. T. Gao, Z. Zhou, J. Y. Yu, D. X. Cao, G. L. Wang, B. Ding and Y. J. Li, All-in-One Compact Architecture toward Wearable All-Solid-State, High-Volumetric-Energy-Density Supercapacitors, *ACS Appl. Mater. Interfaces*, 2018, **10**, 23834–23841, DOI: **10.1021/acsami.8b06143**.

29 Q. F. Liu, L. M. Zang, X. Qiao, J. H. Qiu, X. Wang, L. Hu, J. Yang and C. Yang, Compressible All-In-One Supercapacitor with Adjustable Output Voltage Based on Polypyrrole-Coated Melamine Foam, *Adv. Electron. Mater.*, 2019, **5**, 1900724, DOI: **10.1002/aelm.201900724**.

30 R. Sun, H.-B. Zhang, J. Liu, X. Xie, R. Yang, Y. Li, S. Hong and Z.-Z. Yu, Highly Conductive Transition Metal Carbide/Carbonitride(MXene)@polystyrene Nanocomposites Fabricated by Electrostatic Assembly for Highly Efficient Electromagnetic Interference Shielding, *Adv. Funct. Mater.*, 2017, **27**, 1702807, DOI: **10.1002/adfm.201702807**.

31 A. Lipatov, M. Alhabeb, M. R. Lukatskaya, A. Boson, Y. Gogotsi and A. Sinitskii, Effect of Synthesis on Quality, Electronic Properties and Environmental Stability of Individual Monolayer Ti_3C_2 MXene Flakes, *Adv. Electron. Mater.*, 2016, **2**, 1600255, DOI: **10.1002/aelm.201600255**.

32 J. Li, X. Yuan, C. Lin, Y. Yang, L. Xu, X. Du, J. Xie, J. Lin and J. Sun, Achieving High Pseudocapacitance of 2D Titanium Carbide (MXene) by Cation Intercalation and Surface Modification, *Adv. Energy Mater.*, 2017, **7**, 1602725, DOI: **10.1002/aenm.201602725**.

33 M. Naguib, V. N. Mochalin, M. W. Barsoum and Y. Gogotsi, 25th Anniversary Article: MXenes: A New Family of Two-Dimensional Materials, *Adv. Mater.*, 2014, **26**, 992–1005, DOI: **10.1002/adma.201304138**.

34 X. H. Sang, Y. Xie, M. W. Lin, M. Alhabeb, K. L. Van Aken, Y. Gogotsi, P. R. C. Kent, K. Xiao and R. R. Unocic, Atomic Defects in Monolayer Titanium Carbide ($Ti_3C_2T_x$) MXene, *ACS Nano*, 2016, **10**, 9193–9200, DOI: **10.1021/acsnano.6b05240**.

35 Y. Q. Deng, T. X. Shang, Z. T. Wu, Y. Tao, C. Luo, J. C. Liang, D. L. Han, R. Y. Lyu, C. S. Qi, W. Lv, F. Y. Kang and Q. H. Yang, Fast Gelation of $Ti_3C_2T_x$ MXene Initiated by Metal Ions, *Adv. Mater.*, 2019, **31**, 1902432, DOI: **10.1002/adma.201902432**.

36 J. Li, X. T. Yuan, C. Lin, Y. Q. Yang, L. Xu, X. Du, J. L. Xie, J. H. Lin and J. L. Sun, Achieving High Pseudocapacitance of 2D Titanium Carbide (MXene) by Cation Intercalation and Surface Modification, *Adv. Energy Mater.*, 2017, **7**, 1602725, DOI: **10.1002/aenm.201602725**.

37 X.-D. Zhu, Y. Xie and Y.-T. Liu, Exploring the synergy of 2D MXene-supported black phosphorus quantum dots in hydrogen and oxygen evolution reactions, *J. Mater. Chem. A*, 2018, **6**, 21255–21260.

38 X. T. Gao, Y. Xie, X.-D. Zhu, K. N. Sun, X. M. Xie, Y.-T. Liu, J. Y. Yu and B. Ding, Ultrathin MXene Nanosheets Decorated with TiO2 Quantum Dots as an Efficient Sulfur Host toward Fast and Stable Li-S Batteries, *Small*, 2018, **14**, e1802443.

39 R. Garg, A. Agarwal and M. Agarwal, Synthesis and optimisation of MXene for supercapacitor application, *J. Mater. Sci.: Mater. Electron.*, 2020, **31**, 18614–18626.

40 X. X. Li, Y. N. Ma, P. Z. Shen, C. K. Zhang, J. F. Yan, Y. B. Xia, S. J. Luo and Y. H. Gao, Self-Healing Microsupercapacitors with Size-Dependent 2D MXene, *ChemElectroChem*, 2020, **7**, 821–829.

41 L. Li, D. Chen and G. Z. Shen, All-$Ti_3C_2T_x$ MXene Based Flexible On-chip Microsupercapacitor Array, *Chem. Res. Chin. Univ.*, 2020, **36**, 694–698.

42 L. Weng, F. Y. Qi and Y. G. Min, The $Ti_3C_2T_x$ MXene coated metal mesh electrodes for stretchable supercapacitors, *Mater. Lett.*, 2020, **278**, 128235.

43 N. Kurra, B. Ahmed, Y. Gogotsi and H. N. Alshareef, MXene-on-Paper Coplanar Microsupercapacitors, *Adv. Energy Mater.*, 2016, **6**, 1601372.

44 S. L. Guo, R. H. Zhu, J. W. Chen, W. L. Liu, Y. X. Zhang, J. M. Li and H. Z. Li, MXene-based all-solid flexible electrochromic microsupercapacitor, *Microsyst. Nanoeng.*, 2024, **10**, 89.

45 J. Yan, C. E. Ren, K. Maleski, C. B. Hatter, B. Anasori, P. Urbankowski, A. Sarycheva and Y. Gogotsi, Flexible MXene/Graphene Films for Ultrafast Supercapacitors with Outstanding Volumetric Capacitance, *Adv. Funct. Mater.*, 2017, **27**, 1701264, DOI: **10.1002/adfm.201701264**.

46 M. R. Lukatskaya, O. Mashtalir, C. E. Ren, Y. Dall'Agnese, P. Rozier, P. L. Taberna, M. Naguib, P. Simon, M. W. Barsoum and Y. Gogotsi, Cation Intercalation and High Volumetric Capacitance of Two-Dimensional Titanium Carbide, *Science*, 2013, **341**, 1502–1505, DOI: **10.1126/science.1241488**.

47 X. Q. Xie, M. Q. Zhao, B. Anasori, K. Maleski, C. E. Ren, J. W. Li, B. W. Byles, E. Pomerantseva, G. X. Wang and Y. Gogotsi, Porous heterostructured MXene/carbon nanotube composite paper with high volumetric capacity for sodium-based energy storage devices, *Nano Energy*, 2016, **26**, 513–523, DOI: **10.1016/j.nanoen.2016.06.005**.

48 M. Q. Zhao, C. E. Ren, Z. Ling, M. R. Lukatskaya, C. F. Zhang, K. L. Van Aken, M. W. Barsoum and Y. Gogotsi, Flexible MXene/Carbon Nanotube Composite Paper with High Volumetric Capacitance, *Adv. Mater.*, 2015, **27**, 339–345, DOI: **10.1002/adma.201404140**.

49 J. Acharya, G. P. Ojha, B. S. Kim, B. Pant and M. Park, Modish Designation of Hollow-Tubular rGO-$NiMoO_4$@Ni-Co-S Hybrid Core-shell Electrodes with Multichannel

Superconductive Pathways for High-Performance Asymmetric Supercapacitors, *ACS Appl. Mater. Interfaces*, 2021, **13**, 17487–17500, DOI: **10.1021/acsami.1c00137**.

50 H. Lindström, S. Södergren, A. Solbrand, H. Rensmo, J. Hjelm, A. Hagfeldt and S.-E. Lindquist, Li^+ Ion Insertion in TiO_2 (Anatase). 1. Chronoamperometry on CVD Films and Nanoporous Films, *J. Phys. Chem. B*, 1997, **101**, 7710–7716, DOI: **10.1021/jp970489r**.

51 T. C. Liu, W. G. Pell, B. E. Conway and S. L. Roberson, Behavior of molybdenum nitrides as materials for electrochemical capacitors-Comparison with ruthenium oxide, *J. Electrochem. Soc.*, 1998, **145**, 1882–1888, DOI: **10.1149/1.1838571**.